Davies, J. T., private Communication, 1979, Metal Box Ltd., London.
Garlanda, T.; Masoero, M. *Chim. Ind.* **1966**, *48*(9), 936.
Huang, W., S. B. Thesis, Department of Chemical Engineering, Massachusetts Institute of Technology, Cambridge, MA, 1980.
Masoero, M.; Garlanda, T. *Chim. Ind.* **1965**, *47*(9), 973.
Menting, L. C.; Hoogstad, B.; Thijssen, H. A. C. *J. Food Technol.* **1970**, *5*, 127.
Pfab, von W.; Mücke, G. *Dtsch. Lebensm.-Rundsch.* **1977**, *73*, 1.
Phillips, M. *New Eng. J. Med.* **1979**, *302*(18), 1005.
Reid, R. C.; Sidman, K. R.; Schwope, A. D.; Till, D. E. *Ind. Eng. Chem. Prod. Res. Dev.* **1980**, *19*, 580.
Rudolph, F. B. *J. Polym. Sci. Polym. Phys. Ed.* **1979**, *17*, 1709; **1980**, *18*, 2323.

Received for review April 6, 1981
Accepted February 16, 1982

Supplementary Material Available: Five detailed tables showing migration data for styrene monomer to foods and FSL (5 pages). Ordering information is given on any current masthead page.

Downstream Development of Two-Dimensional Viscocapillary Film Flow

Brian G. Higgins*

Department of Chemical Engineering and Material Science, University of Minnesota, Minneapolis, Minnesota 55455

Downstream development of two-dimensional, steady liquid film flow on a moving horizontal substrate is analyzed by linearizing the Navier–Stokes system for small departures from the asymptotic plug flow. The linearized system is reduced to an eigenproblem which is solved in closed form for all Reynolds and capillary numbers. Although each eigensolution describes a successively more complicated motion which decays with distance downstream, it is shown that sufficiently far downstream the slowest decaying mode accurately predicts the dynamic behavior of the liquid film at each section along the flow. From this information can be derived vector Robin boundary conditions on flow upstream of such a section. The application of these boundary conditions in numerical simulation of free surface flows when the out-flow boundary conditions are known only asymptotically is discussed.

1. Introduction

The common practice in numerical simulations, whether finite difference or finite element, when conditions specified at an open-flow boundary are known asymptotically is to apply them at some finite location. The sensitivity of the simulation to the locations of the *stand-in* flow boundaries has to be tested, however. In practice this is usually done by moving the boundaries away from the region of central interest until the sensitivity of the simulation to locations of the stand-in boundaries is acceptably small. How far the stand-in boundaries have to be located depends on whether the boundary conditions applied at them are Dirichlet, Neumann, or Robin conditions. Generally Dirichlet conditions (fixing the dependent variables) have to be specified furthest away and Neumann conditions (fixing the derivatives of dependent variables) next furthest. Robin conditions (relating dependent variables to their derivatives) when available can be specified rather closer.

In numerical simulation of steady liquid film flow, the conditions at the downstream out-flow boundary are typically imposed as Dirichlet or Neumann conditions derived from the asymptotic rectilinear flow (Silliman 1979, Saito and Scriven 1981). The purpose of this paper to to derive expressions for the velocity and free surface shape that accurately predict the dynamics of the liquid film as it approaches its downstream asymptotic flow regime, and to demonstrate how vector Robin conditions which relate velocity to momentum flux and location to slope of the free surface at the out-flow boundary can be constructed from them.

The geometrical configuration considered is shown in Figure 1. Liquid is extruded from a slot onto a fast-moving substrate. Downstream of the slot exit the liquid film accelerates in speed, diminishes in thickness, and approaches a state of uniform thickness with uniform velocity. (When the substrate moves slowly or not at all, the film decelerates and thickens, but this case is not considered here.) The rate of approach depends on the volumetric extrusion rate of liquid, the substrate speed, and liquid properties including surface tension. If the substrate is inclined over distances greater than the capillary length, the gravititional body force may be significant. In this paper, however, attention is confined to liquid film on a moving *horizontal* substrate. Then, parameters which characterize the approach can be grouped into two dimensional numbers: a Reynolds number which measures the relative importance of inertial forces to viscous forces in the liquid film, and a capillary number which measures the relative importance of viscous forces to capillary pressure, the effect of surface tension in a curved meniscus.

The effect of capillary number has been addressed before. Coyne and Elrod (1969) examined the final development of a liquid film formed in a partially submerged lubricating bearing, a physical situation similar to that shown in Figure 1. Their work appears to have been inspired by that of Cox (1962), who analyzed the shape of the liquid film left behind when a long bubble is forced through a tube containing a viscous fluid. Coyne and Elrod's (1969) results are vitiated, however, by an error in the characteristic equation they derived for computing the eigenvalues which describe the development of the liquid film. This point is discussed further in section 4. In another work that parallels Cox's, Groenveld and van Dortmund (1970) studied the development of the liquid film formed in dip-coating. They include the effect of gravity but report results only for infinitely large capillary numbers. None of these authors accounts for the inertia of the developing liquid film, all of them having assumed

* The Institute of Paper Chemistry, P.O. Box 1039, Appleton, WI 54912.

0196-4313/82/1021-0168$01.25/0

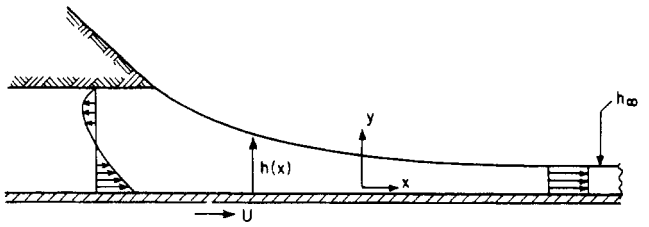

Figure 1. Downstream development of film flow on a moving substrate.

that the Reynolds number is sufficiently small that the liquid motion can be described by the creeping-flow equations.

Ruschak (1974) analyzed the very same configuration shown in Figure 1. His analysis is based on perturbation from the limiting static meniscus which the free surface approaches as the substrate speed tends to zero and it does not account for liquid inertia. Recently, Silliman (1979) solved the Navier–Stokes system for two-dimensional film flow by the finite element method for a variety of upstream velocity profiles in the slot, and for various combinations of Reynolds and capillary numbers. He calculated free surface shapes and velocity fields of liquid films such as those treated here. In each case he found that beyond a certain distance downstream of the contact line the film thickness diminishes exponentially toward the asymptotic thickness.

In section 2 the Navier–Stokes system is linearized for small departures from the asymptotic downstream plug flow. The linearized system is reduced to an eigenproblem of which each eigensolution describes a successively more complicated motion, all of them decaying with distance downstream. What is most relevant to the development process is the mode that decays slowest, i.e., the eigensolution having the eigenvalue with the smallest real part. The rate the free surface relaxes is also described by the same eigensolution. The procedure used in section 2 to construct the eigenproblem resembles Wilson's (1969) method for analyzing the development of Poiseuille flow in a slot.

In section 3 the eigenproblem is solved in closed form. It turns out that when the Reynolds number is zero, the eigenvalue spectrum consists of one real eigenvalue and an infinite sequence of complex eigenvalues. Of the lot, the real eigenvalue has the smallest real part. For Reynolds numbers greater than zero the eigenvalue with the smallest real part is again real, but the remaining spectrum consists of real and complex eigenvalues.

In section 4 the results are compared with Silliman's (1979) finite element solutions. The conclusion is that slowest decaying mode accurately predicts velocity and pressure fields and the shape of the free surface at each section of the flow one to two slot widths downstream of the contact line. Finally, it is shown that a vector Robin boundary condition on flow upstream of such a section can be constructed from the slowest decaying eigensolution; the proportionality constant in the Robin condition turns out to be the eigenvalue with the smallest real part.

2. Mathematical Formulation

The liquid motion is taken to be steady and two-dimensional. If $\psi \equiv \hat{\psi}/Uh_\infty$ represents the dimensionless stream function, $\hat{\psi}$ being its dimensional counterpart, the components of velocity are

$$u \equiv \frac{\partial \psi}{\partial y}; \quad v \equiv -\frac{\partial \psi}{\partial x} \tag{2.1}$$

Here $x \equiv \hat{x}/h_\infty$ and $y \equiv \hat{y}/h_\infty$ are dimensionless Cartesian coordinates oriented as in Figure 1; h_∞ is the final film thickness and U is the substrate speed.

For a Newtonian liquid the equation of motion in dimensionless form is

$$N_{\mathrm{Re}}\left(\psi_y\frac{\partial}{\partial x} - \psi_x\frac{\partial}{\partial y}\right)\nabla^2\psi = \nabla^4\psi \tag{2.2}$$

where the Reynolds number is $N_{\mathrm{Re}} \equiv \rho U h_\infty/\mu$, ρ being the density and μ the viscosity. The subscripts x and y denote partial differentiation. At the liquid surface in contact with a tenuous gas-phase the appropriate form of the dimensionless normal stress boundary condition is (*cf.* Higgins et al. 1977)

$$\frac{1}{N_{\mathrm{ca}}}\frac{\mathrm{d}}{\mathrm{d}x}\left\{\frac{\mathrm{d}^2h}{\mathrm{d}x^2}\Big/\left[1+\left(\frac{\mathrm{d}h}{\mathrm{d}x}\right)^2\right]^{3/2}\right\} + \psi_{yyy} + 3\psi_{xxy} - N_{\mathrm{Re}}(\psi_y\psi_{yx} - \psi_x\psi_{yy}) + \frac{\mathrm{d}h}{\mathrm{d}x}(2\psi_{xyy} - 2\psi_{xxx}) + N_{\mathrm{Re}}\frac{\mathrm{d}h}{\mathrm{d}x}(\psi_y\psi_{xx} - \psi_x\psi_{xy}) + \left(\frac{\mathrm{d}h}{\mathrm{d}x}\right)^2(\psi_{yyy} - \psi_{yxx}) + 4\psi_{yx}\left(\frac{\mathrm{d}h}{\mathrm{d}x}\right)\frac{\mathrm{d}^2h}{\mathrm{d}x^2}\Big/\left[1-\left(\frac{\mathrm{d}h}{\mathrm{d}x}\right)^2\right] = 0 \tag{2.3}$$

and the dimensionless shear stress boundary condition is that for vanishing shear stress

$$\left[1-\left(\frac{\mathrm{d}h}{\mathrm{d}x}\right)^2\right](\psi_{yy} - \psi_{xx}) - 4\frac{\mathrm{d}h}{\mathrm{d}x}\psi_{yx} = 0 \tag{2.4}$$

Here $h \equiv \hat{h}/h_\infty$ is the local dimensionless film thickness and $N_{\mathrm{ca}} \equiv \mu U/\sigma$ is the capillary number. The surface tension, σ, is taken to be sensibly constant and the gas-phase pressure level is set to zero. The remaining boundary condition to be satisfied at the free surface is the kinematic condition

$$\psi_y\frac{\mathrm{d}h}{\mathrm{d}x} = -\psi_x \tag{2.5}$$

At the moving substrate there is neither slip, penetration, nor void

$$\psi_y = 1; \quad \psi_x = 0 \tag{2.6}$$

The requirement that the velocity become uniform sufficienty far downstream implies

$$\psi_y \to 1; \quad \psi_x \to 0; \quad h(x) \to 1 \text{ as } x \to \infty \tag{2.7}$$

Finally there must be a boundary condition upstream. At an arbitrarily chosen place, $x = 0$, one might suppose the velocity distribution and film thickness are known

$$\psi_y = f(y); \quad \psi_x = g(y); \quad h(0) = d \quad (\text{at } x = 0) \tag{2.8}$$

If the location $x = 0$ is chosen sufficiently far downstream of the separation line, or contact line of the meniscus with the slot edge, the upstream condition can be written (cf. Wilson, 1969)

$$\psi_y(0,y) = 1 + \epsilon f(y); \quad \psi_x(0,y) = \epsilon g(y); \quad h(0) = 1 + \epsilon d \quad (\text{at } x = 0) \tag{2.9}$$

The parameter ϵ is proportional to the inclination of the free surface at $x = 0$ and can be made as small as required by choosing $x = 0$ sufficiently far downstream of the separation line.

To analyze the final development of the liquid film, we linearize the set of eq 2.2 to 2.9 around the downstream asymptotic profile (2.7). The appropriate perturbation equations are found with an old method formalized by Joseph and Fosdick (1973). The basic postulate, which is

backed by a century of success, is that the dependent variables (ψ, h) can be represented by power series in ϵ

$$\begin{bmatrix}\psi(x, y; \epsilon)\\ h(x; \epsilon)\end{bmatrix} = \sum_{p=0}^{\infty} \frac{\epsilon^p}{p!}\begin{bmatrix}\psi^{(p)}(x, y)\\ h^{(p)}(x)\end{bmatrix} \quad (2.10)$$

Substituting (2.10) into (2.2)–(2.9) and collecting terms of like order in ϵ yields a sequence of linear partial differential equations and boundary conditions for the functions $\psi^{(p)}$ and $h^{(p)}$. The zeroth-order solution is the asymptotic downstream flow

$$\psi_y^{(0)} = 1; \quad \psi_x^{(0)} = 0; \quad h^{(0)} = 1 \quad (2.11)$$

The first-order terms must satisfy

$$N_{Re}\psi_y^{(0)}\frac{\partial}{\partial x}\nabla^2\psi^{(1)} = \nabla^4\psi^{(1)} \quad (2.12)$$

$$\psi^{(1)} = 0; \quad \psi_y^{(1)} = 0; \quad (\text{at } y = 0) \quad (2.13)$$

$$\psi_{yy}^{(1)} - \psi_{xx}^{(1)} = 0 \quad (2.14)$$

$$\frac{1}{N_{ca}}\frac{d^3h^{(1)}}{dx^3} + \psi_{yyy}^{(1)} + 3\psi_{xxy}^{(1)} - N_{Re}\psi_y^{(0)}\psi_{yx}^{(1)} = 0 \quad (\text{at } y = 1) \quad (2.15)$$

$$\psi_y^{(0)}\frac{dh^{(1)}}{dx} + \psi_x^{(1)} = 0 \quad (2.16)$$

$$\psi_x^{(1)}, \psi_y^{(1)} \to 0 \quad (\text{as } x \to \infty) \quad (2.17)$$

The normal stress boundary condition's dependence on $h(x)$ can be removed with the kinematic condition (2.16). If the stream function $\psi^{(1)}$ is expanded in exponentially decaying functions of the downstream distance, vis.

$$\psi^{(1)}(x, y) = \sum_{n=0}^{\infty} D_n\phi_n(y)e^{\alpha_n x} \quad (2.18)$$

the first-order equations (2.12)–(2.15) become the following eigenproblem (primes denote differentiation with respect to y)

$$\phi_n'''' + 2\alpha_n^2\phi_n'' + \alpha_n^4\phi_n - \alpha_n N_{Re}(\phi_n'' + \alpha_n^2\phi_n) = 0 \quad (2.19)$$

$$\phi_n(0) = \phi_n'(0) = 0 \quad (2.20)$$

$$\phi_n''(1) - \alpha_n^2\phi_n(1) = 0 \quad (2.21)$$

$$\phi_n'''(1) + 3\alpha_n^2\phi_n'(1) - \alpha_n^3\phi_n(1)/N_{ca} - \alpha_n N_{Re}\phi_n'(1) = 0 \quad (2.22)$$

The perturbation of the free surface is

$$h^{(1)} = -\sum_{n=0}^{\infty} D_n\phi_n(1)e^{\alpha_n x} \quad (2.23)$$

The eigenvalues α_n are, in general, complex and for each fixed N_{Re} and N_{ca} there is an infinite sequence of them. Each eigenfunction $\phi_n(y)$ corresponds to successively more complicated motions in the liquid film. The infinite set of complex coefficients D_n in (2.18) must be so chosen as to satisfy the upstream condition at $x = 0$; that is

$$\psi_y^{(1)}(0,y) \equiv f(y) = \text{real}\sum_{n=0}^{\infty} D_n\phi_n'(y) \quad (2.24)$$

$$\psi_x^{(1)}(0,y) \equiv g(y) = \text{real}\sum_{n=0}^{\infty} D_n\alpha_n\phi_n(y) \quad (2.25)$$

Note, the boundary value problem (2.19)–(2.22) is nonselfadjoint; consequently, the eigenfunctions ϕ_n do not in general form an orthogonal set on the interval [0,1], which means that an appropriate expansion theorem for determining the D_n's must be found. This issue will not be pursued here because the location $x = 0$ is specified downstream of the contact line and thus $f(y)$ and $g(y)$ are in general unknown. (If $f(y)$ and $g(y)$ are known, methods based on biorthogonal expansions as described by Joseph and Sturges (1975) and Kumar and Yanik (1980) can be used.) However, what is of interest here are the eigenvalues; they determine the decay rates of the corresponding eigensolutions.

Table I. Dependence of $\tilde{\alpha}_0$ and $\tilde{\alpha}_1$ on N_{ca}; $\tilde{\alpha}_1$ Is the Complex Root of Eq 3.4 with the Smallest Real Part

N_{ca}	$\tilde{\alpha}_0$	$\tilde{\alpha}_1$
1000	−0.7390	−2.4872 ± 1.8096i
10	−0.7342	−2.5190 ± 1.8269i
1	−0.6969	−2.7935 ± 1.9069i
0.1	−0.5287	−3.5115 ± 1.6288i
0.01	−0.2936	−3.7201 ± 1.4176i

3. Solution to the Eigenproblem

When the Reynolds number is so small as to be sensibly zero, the eigenproblem (2.19)–(2.22) simplifies to

$$\tilde{\phi}_n'''' + 2\tilde{\alpha}_n^2\tilde{\phi}_n'' + \tilde{\alpha}_n^4\tilde{\phi}_n = 0 \quad (3.1)$$

$$\tilde{\phi}_n(0) = \tilde{\phi}_n'(0) = 0$$

$$\tilde{\phi}_n''(1) - \tilde{\alpha}_n^2\tilde{\phi}_n(1) = 0 \quad (3.2)$$

$$\phi_n'''(1) + 3\tilde{\alpha}_n^2\tilde{\phi}_n'(1) - \frac{\tilde{\alpha}_n^3}{N_{ca}}\tilde{\phi}_n(1) = 0$$

The tilde denotes the limit $N_{Re} = 0$. The eigenfunctions $\tilde{\phi}_n$ that satisfy (3.1) and (3.2) are

$$\tilde{\phi}_n(y) = (\cos\tilde{\alpha}_n - \tilde{\alpha}_n\sin\tilde{\alpha}_n)\sin\tilde{\alpha}_n y - (\tilde{\alpha}_n^2\cos\tilde{\alpha}_n)y\sin\tilde{\alpha}_n y + (\tilde{\alpha}_n^2\sin\tilde{\alpha}_n - \tilde{\alpha}_n\cos\tilde{\alpha}_n)y\cos\tilde{\alpha}_n y \quad (3.3)$$

where the eigenvalues $\tilde{\alpha}_n$ ($n = 0, 1, 2, \cdots$) are the roots of

$$2\cos^2\tilde{\alpha}_n - 2\tilde{\alpha}_n^2 + \frac{1}{N_{ca}}(\tilde{\alpha}_n - \cos\tilde{\alpha}_n\sin\tilde{\alpha}_n) = 0 \quad (3.4)$$

The eigenvalues are in general complex and are numbered in a sequence corresponding to increasing size of their real parts. Further, to ensure that $\psi^{(1)}$ tends to zero as x becomes large, the roots of (3.4) that can be accepted are those that have negative real parts.

The roots of (3.9) were computed numerically (details are given in Higgins, 1980). The eigenvalue with the smallest real part, $\tilde{\alpha}_0$, turns out to be real. The remaining eigenvalues in the spectrum are complex. In Table I the real eigenvalue, $\tilde{\alpha}_0$, and the complex eigenvalue with the smallest real part, $\tilde{\alpha}_1$, are tabulated as functions of N_{ca}. The largest negative value that $\tilde{\alpha}_0$ attains is −0.7390, which occurs when N_{ca} is infinite. In contrast, the real part of $\tilde{\alpha}_1$ attains its largest negative value, namely −3.7488, when N_{ca} is zero. The asymptotic behavior of the real root $\tilde{\alpha}_0$ as N_{ca} approaches zero can be found by expanding $\tilde{\alpha}_0$ in a power series in N_{ca}

$$\tilde{\alpha}_0 \sim N_{ca}^p\tilde{\alpha}_0^{(1)} + N_{ca}^q\tilde{\alpha}_0^{(2)} + \cdots \quad (3.5)$$

Substituting this series into (3.4) and collecting terms of like power in N_{ca} yields

$$\tilde{\alpha}_0^{(1)} = -3^{1/3}; \quad p = 1/3 \quad (3.6)$$

Thus

$$\tilde{\alpha}_0 \to -(3N_{ca})^{1/3} \text{ as } N_{ca} \to 0 \quad (3.7)$$

The limiting form of the eigenfunction $\tilde{\phi}_0(y)$ as $N_{ca} \to 0$

Table II. Dependence of α_0 on N_{ca} and N_{Re}

	N_{Re}			
N_{ca}	0.1	1.0	10	100
1000	−0.72901	−0.64317	−0.22569	−0.02464
10	−0.72447	−0.64003	−0.22562	−0.02464
1	−0.68836	−0.61433	−0.22491	−0.02464
0.1	−0.52444	−0.48603	−0.21850	−0.02464
0.01	−0.29249	−0.28170	−0.18292	−0.02463

is found by expanding the expression for the eigenfunction, (3.3), for small $\tilde{\alpha}_0$; this yields

$$\tilde{\phi}_0(y) \sim \tilde{\alpha}_0{}^3\left(\frac{y^3}{3} - y^2\right) \tag{3.8}$$

Thus in the limit $N_{ca} \to 0$, the streamwise velocity component corresponding to $\tilde{\phi}_0(y)$ is a locally varying Poiseuille flow driven by a capillary pressure gradient.

When the Reynolds number is not zero, the general solution of (2.19) can be easily found as the sum of $\phi_n \equiv \phi_{nI} + \phi_{nR}$, where ϕ_{nI} and ϕ_{nR} satisfy

$$\phi_{nI}'' + \alpha_n{}^2\phi_{nI} = 0;\ \phi_{nR}'' + \lambda_n{}^2\phi_{nR} = 0 \tag{3.9a,b}$$

respectively. The parameter λ_n is related to the eigenvalue α_n by

$$\lambda_n{}^2 \equiv \alpha_n{}^2 - \alpha_n N_{Re} \tag{3.10}$$

It is noteworthy that a decomposition of $\phi_n \equiv \phi_{nI} + \phi_{nR}$ is equivalent to separating the flow into an irrotational part given by

$$\psi_I \equiv C_n e^{\alpha_n x}\phi_{nI}(y), \text{ where } \nabla^2\psi_I = 0 \tag{3.11}$$

and a rotational part given by

$$\psi_R \equiv C_n e^{\alpha_n x}\phi_{nR}(y), \text{ where } \left(\nabla^2 - N_{Re}\frac{\partial}{\partial x}\right)\psi_R = 0 \tag{3.12}$$

The eigenfunctions $\phi_n(y)$ that satisfy (3.9) and boundary conditions (2.20–2.22) are

$$\phi_n(y) = C_{1n}\cos\alpha_n y + C_{2n}\sin\alpha_n y + C_{3n}\cos\lambda_n y + C_{4n}\sin\lambda_n y \tag{3.13}$$

where

$$C_{1n} \equiv (\lambda_n{}^2 + \alpha_n{}^2)\sin\lambda_n + 2\lambda_n\alpha_n\sin\alpha_n$$

$$C_{2n} \equiv -\frac{\lambda_n}{\alpha_n}(\lambda_n{}^2 + \alpha_n{}^2)\cos\lambda_n + 2\lambda_n\alpha_n\cos\alpha_n$$

$$C_{3n} \equiv -C_{1n};\quad C_{4n} \equiv -\frac{\alpha_n}{\lambda_n}C_{2n} \tag{3.14}$$

The eigenvalues α_n are the roots of

$$(A_n + B_n)\cos(\alpha_n - \lambda_n) - (A_n - B_n)\cos(\alpha_n + \lambda_n) + \frac{\alpha_n N_{Re}}{\lambda_n N_{ca}}(\alpha_n + \lambda_n)\sin(\alpha_n - \lambda_n) - \frac{\alpha_n N_{Re}}{\lambda_n N_{ca}}(\alpha_n - \lambda_n)\sin(\alpha_n + \lambda_n) - 4(2\alpha_n{}^2 - \alpha_n N_{Re}) = 0 \tag{3.15}$$

where

$$A_n \equiv 8\alpha_n\lambda_n + \alpha_n N_{Re}{}^2/\lambda_n$$

$$B_n \equiv 4(2\alpha_n{}^2 - \alpha_n N_{Re}) + N_{Re}{}^2 \tag{3.16}$$

It is evident from (3.10), the defining equation for λ_n, that as N_{Re} approaches zero the parameter λ_n approaches α_n, which in turn makes the left side of (3.15) approach zero. Consequently, in the limit $N_{Re} = 0$, the eigenvalues must be found either by applying l'Hospital's rule to (3.15) or by using (3.4).

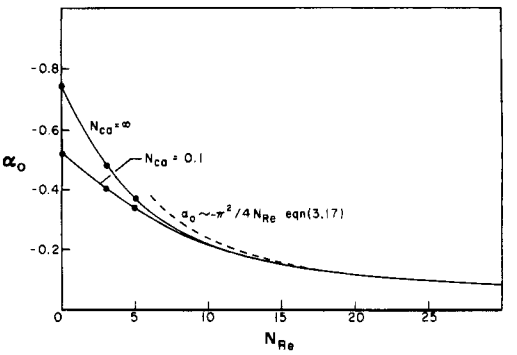

Figure 2. The dependence of α_0 on N_{Re} and N_{ca}; (●), value of α_0 calculated from Silliman's (1979) finite element solutions.

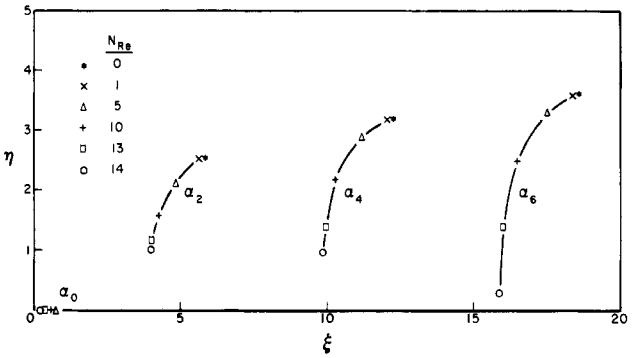

Figure 3. Representative trajectories of eigenvalues, $\alpha_n \equiv \xi_n + \eta_n i$, in the complex plane; $N_{ca} = \infty$.

Table II summarizes the dependence of α_0, the eigenvalue with the smallest real part, on N_{ca} and N_{Re}. Again, α_0 is real and for fixed N_{ca} decreases with increasing N_{Re}. The asymptotic value α_0 approaches as N_{Re} becomes large is found by taking the limit $N_{Re} \to \infty$ in (3.15) and noting that $\alpha_0 \sim -\lambda_0{}^2/N_{Re}$ in this limit. The result is

$$\alpha_0 \sim -\pi^2/4N_{Re} \text{ as } N_{Re} \to \infty \tag{3.17}$$

The limiting form of the eigenfunction $\phi_0(y)$ when $N_{Re} \to \infty$ is

$$\phi_0(y) \sim \frac{\pi^2}{4}\left(1 - \cos\frac{\pi y}{2}\right) \tag{3.18}$$

Thus in this limit the streamwise velocity component corresponding to ϕ_0 is a half sinefunction.

In Figure 2, α_0 is plotted as a function of N_{Re} for different values of N_{ca}. Figure 2 shows that when $N_{Re} > 12$, α_0 is insensitive to variations in N_{ca} and is well approximated by its asymptotic value $\alpha_0 \sim -\pi^2/4N_{Re}$ (the dashed curve in Figure 2). The effect of N_{ca} is, as expected, most pronounced when N_{Re} is much less than unity.

The eigenvalues other than α_0 behave quite differently. When N_{Re} is zero, the α_n's are complex and as N_{Re} is increased they approach the real axis: see Figure 3. The eigenvalues with the largest negative real parts approach the most rapidly. Numerical calculations showed that for $N_{Re} = 100$ the real part of α_1 is still approximately an order of magnitude larger than α_0.

4. Discussion

The analysis detailed above shows that the approach to the asymptotic plug flow is described by an infinite set of eigensolutions which decay with distance downstream of the contact line. Because the eigenvalue with the smallest real part, α_0, is at least an order of magnitude smaller than any other eigenvalue in the spectrum, it is expected that with increasing distance downstream, the approach is eventually described by the eigensolution corresponding

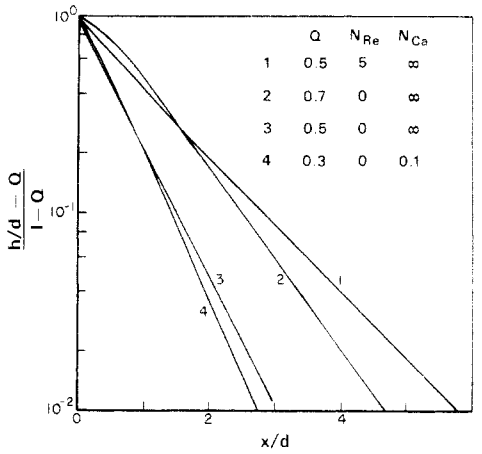

Figure 4. Semilog plot of meniscus profile as a function of position (Silliman 1979). The profiles are normalized with the slot width d; Q is the final film thickness divided by the slot width.

to α_0. When all the eigensolutions other than $D_0e^{\alpha_0 x}\phi_0(y)$ are discarded from the power series expansion for the stream function and free surface shape, (2.10), the approach to plug flow is described by

$$\psi(x,y) \sim y + \epsilon D_0 e^{\alpha_0 x}\phi_0(y) \quad (4.1a)$$

$$h(x) \sim 1 + \epsilon D_0 e^{\alpha_0 x}\phi_0(1) \quad (\text{as } x \to \infty) \quad (4.1b)$$

The eigenvalue α_0 is always real (see Table II); hence the velocity field and film thickness decay exponentially toward their respective asymptotic values. Silliman's (1979) finite element solutions confirm this behavior. In Figure 4 free surface profiles computed by Silliman (1979) are plotted on semilog coordinates for various Reynolds and capillary numbers. It is evident from the plots that except for a distance of one to two slot-widths downstream of the contact line the profiles are straight lines.

Values of α_0 calculated from Silliman's (1979) profiles are plotted in Figure 3 along with values of α_0 calculated from the characteristic equation (3.15). The agreement is within half a percent. More extensive numerical studies carried out by Saito and Scriven (1981) also confirm predictions of α_0 given here. Thus the slowest decaying eigensolution accurately predicts the dynamics of the liquid film one to two slotwidths downstream of the contact line.

The values of α_0 calculated by Coyne and Elrod (1969) for the case $N_{Re} = 0$ do not agree with values of $\tilde{\alpha}_0$ presented in Table I. The cause for the discrepency is traced to an incorrect characteristic equation used by Coyne and Elrod for calculating $\tilde{\alpha}_0$. According to eq 16 of their paper

$$-2\left(\tilde{\alpha}_n^2 + \tilde{\alpha}_n \sin\tilde{\alpha}_n - \tilde{\alpha}_n\frac{\sin 2\tilde{\alpha}_n}{2} - \cos\tilde{\alpha}_n\right) + \frac{1}{N_{ca}}(\tilde{\alpha}_n - \cos\tilde{\alpha}_n \sin\tilde{\alpha}_n) = 0 \quad (4.2)$$

This disagrees with (3.4) because of an algebraic error made by the authors when they applied the normal stress boundary condition, (2.15).

Boundary Conditions. In numerical simulation of the flows considered here the asymptotic plug flow regime (2.7) is ordinarily accounted for by specifying either Dirichlet conditions

$$\mathbf{v} = \mathbf{i},\ h = 1 \quad (\text{at } x = x_0) \quad (4.3)$$

or Neumann conditions

$$\mathbf{n}\cdot\nabla\mathbf{v} = 0,\ \mathbf{n}\cdot\nabla_{II}h = 0 \quad (\text{at } x = x_0) \quad (4.4)$$

on the velocity and free surface shape at a chosen out-flow boundary. (Instead of (4.4), a traction condition may sometimes be preferred; see Bixler and Scriven, 1980). Here $\mathbf{n}$ is the outward directed unit normal to the out-flow boundary (the unit vector $\mathbf{i}$ in this case), ∇_{II} is the two-dimensional surface gradient operator, and x_0 is the location of the out-flow boundary. As a rule, Neumann conditions represent more of the asymptotic plug flow than do Dirichlet conditions, for a given level of accuracy.

Instead of specifying Neumann or Dirichlet conditions at the out-flow boundary, one may also specify relationships between the dependent variables and their derivatives, i.e., Robin conditions

$$\mathbf{n}\cdot\nabla\mathbf{v} = \boldsymbol{K}\cdot(\mathbf{v} - \mathbf{i}) \quad (\text{at } x = x_0) \quad (4.5a)$$

$$\mathbf{n}\cdot\nabla_{II}h = k(h - 1) \quad (\text{at } x = x_0) \quad (4.5b)$$

But this requires knowledge of the proportionality constants $\boldsymbol{K}$ and k. Because the asymptotic solution (4.1) accurately predicts the velocity and free surface shape at each section along the flow, it must satisfy the Robin conditions (4.5) when the location of the out-flow boundary, x_0, is in the range of validity of the asymptotic solution (4.1). The requirement that (4.1) satisfy (4.5) allows $\boldsymbol{K}$ and k to be determined. Although more than one set of values for $\boldsymbol{K}$ and k can be found, there is a set that is independent of the coefficient D_0, the last vestige of the upstream boundary condition; the set is

$$\boldsymbol{K} = \alpha_0\boldsymbol{I};\quad k = \alpha_0 \quad (4.6)$$

Figure 4 shows that it is permissible to specify (4.5) and stand-in boundary conditions one to two slot-widths downstream of the contact line. Further, α_0 is independent of upstream conditions; it depends on capillary and Reynolds number only. Although Huh and Scriven (1969) and Orr et al. (1977) have successfully demonstrated how asymptotic solutions can be used for calculating static menisci of unbounded extent, this philosophy has only recently been attempted in numerical simulation of free surface flow problems (Bixler and Scriven, 1980).

Acknowledgment

The author would like to thank Professor L. E. Scriven and N. E. Bixler for helpful discussions and criticisms. This research was supported by a National Science Foundation Grant to Professor L. E. Scriven.

Nomenclature

A_n, B_n = constants defined by eq 3.16
C_{in} = constants defined by eq 3.14
D_n = complex coefficients in expansion (2.18)
d = film thickness at $x = 0$, m
h_∞ = final film thickness, m
h = dimensionless local film thickness
N_{ca} = capillary number, $\mu U/\sigma$
N_{Re} = Reynolds number, $\rho U h_\infty/\mu$
U = substrate speed, m/s
u, v = dimensionless velocity components
x, y = dimensionless coordinates

Greek Letters

α_n = complex eigenvalue, $\xi_n + i\eta_n$
λ_n = parameter defined by eq 3.10
ρ = density, kg/m^3
μ = viscosity coefficient, Pa s
σ = surface tension coefficient, N/m
ψ = dimensionless stream function
ϕ_n = dimensionless eigenfunction
ϵ = perturbation parameter defined by eq 2.9

Literature Cited

Bixler, N. E.; Scriven, L. E. *Bull. Am. Phys. Soc.* **1980**, *25*, 1079.
Coyne, J. C.; Elrod, H. G. *J. Lubr. Technol.* **1969**, *91*, 651.
Cox, G. B. *J. Fluid Mech.* **1962**, *14*, 81.
Groenveld, P.; van Dortmund, R. A. *Chem. Eng. Sci.* **1970**, *25*, 1571.

Higgins, B. G.; Silliman, W. J.; Brown, R. A.; Scriven, L. E. *Ind. Eng. Chem. Fundam.* **1977**, *16*, 393.
Higgins, B. G. Ph.D. Thesis, University of Minnesota, Minneapolis, MN, 1980.
Huh, C.; Scriven, L. E. *J. Colloid Interface Sci.* **1969**, *30*, 323.
Joseph, D. D.; Fosdick, R. L. *Arch. Rational. Mech. Anal.* **1973**, *49*, 321.
Joseph, D. D.; Sturges, L. *J. Fluid Mech.* **1975**, *69*, 565.
Kumar, A.; Yajnik, K. S. *J. Fluid Mech.* **1980**, *97*, 27.
Orr, F. M., Jr.; Brown, R. A.; Scriven, L. E. *J. Colloid* Interface *Sci.* **1977**, *60*, 137.
Ruschak, K. J. Ph.D. Thesis, University of Minnesota, Minneapolis, MN, 1974.
Saito, H.; Scriven, L. E. *J. Comput. Phys.* **1981**, *42*, 53.
Silliman, W. J. Ph.D. Thesis, University of Minnesota, Minneapolis, MN, 1979.
Wilson, S. *J. Fluid Mech.* **1969**, *38*, 793.

Received for review January 23, 1981
Revised manuscript received August 3, 1981
Accepted February 1, 1982

EXPERIMENTAL TECHNIQUES

Modified Sealed-Tube Method for the Determination of Critical Temperature

Edilberto Mogollon and Webster B. Kay*

Department of Chemical Engineering, Ohio State University, Columbus, Ohio 43210

Amyn S. Teja

School of Chemical Engineering, Georgia Institute of Technology, Atlanta, Georgia 30332

A modified sealed-tube method for the determination of the critical temperatures of pure fluids and fluid mixtures is described. Critical temperatures of ten normal alkanes from *n*-octane to *n*-heptadecane have been determined and compared with values found in the literature. The method is capable of yielding data of high precision and is suitable for the study of thermally unstable compounds.

Introduction

The determination of the critical temperature of a pure compound or mixture by heating a sample in a sealed glass tube until the liquid–vapor interface is replaced by an opalescent band is commonly referred to as the "sealed-tube" method. It is a relatively simple technique which requires only that the amount of sample enclosed be such that its volume at the critical temperature be equal to the volume of the sealed tube and is capable of yielding data of high precision (Ambrose et al., 1957, 1960, 1962; Cheng et al., 1962).

Modifications to the design of the furnace and of the sealed tube have been made which make it suitable for the study of thermally unstable compounds. In this report, the apparatus and procedure are described and results of the determination of the critical temperatures of the *n*-alkanes from *n*-octane to *n*-heptadecane are presented.

Experimental Section

Apparatus. The furnace was constructed by the Ace Glass Co. and consisted of a quartz tube 5.5 cm in diameter and 46.8 cm long surrounded by a Pyrex glass tube of 9.0 cm diameter. A metallic film of controlled thickness was deposited on the outside surface of the quartz tube. This served as the electrical resistor of the furnace. The current was regulated by means of an autotransformer with a voltage regulator to maintain a constant power supply. With a power input of 750 W, a temperature of 857 K could be maintained. Two diametrically opposed windows 6.5 cm long and 0.32 cm wide and a third window of the same size at 90° to the axis of the other two were provided in order to observe the sample during the heating process. The top of the furnace was closed by a loose-fitting aluminum plug; the bottom was closed by a Teflon plug with an O-ring to ensure a tight fit. The plugs were drilled to take a 0.64 cm diameter stainless steel tube which served as a support for the sealed tube. The furnace was mounted on a trunion and rotated through 90° to provide mixing of the sample during the heating period.

The glass ampule for holding the sample is shown in Figure 1. It was constructed from borosilicate glass tubing (0.55 cm i.d. with a 0.2 cm wall thickness) and was provided with a small well about 5.1 cm deep at one end into which an iron–constantan thermocouple was inserted. The thermocouple output was recorded continuously by means of a Leeds and Northrup Speedomax H recorder with a chart speed of 30.5 cm/min and with a sensitivity equivalent to 0.02 K. The thermocouple was calibrated over the range 475 to 975 K by comparison with an NBS certified platinum thermometer.

Figure 2 shows the sealed tube and thermocouple assembly. E is the stainless steel tube to which the glass tube G and aluminum cap C are attached by clamps B. The thermocouple A enclosed in a ceramic tube D was inserted

0196-4313/82/1021-0173$01.25/0